Automatic Control Loop Tuning for Permanent-Magnet AC Servo Motor Drives

Sheng-Ming Yang, *Member, IEEE*, and Kuang-Wei Lin

***Abstract*—Servo motor drives generally consist of current, velocity, and position control loops. Tuning these controllers to achieve satisfactory and consistent dynamic responses is crucial. In this paper, a parameter identification and autotuning scheme for permanent-magnet ac servo motor drives is presented. Motor electrical parameters such as resistance and inductances were identified first for current control loop tuning. The torque constant and mechanical parameters were then identified for velocity and position loop tuning. The experimental results verified that the proposed scheme can estimate parameters accurately and within a short time. In addition, the system tuned by the proposed scheme was consistent with the desired dynamic performance.**

***Index Terms*—AC servo motor drives, autotune, parameter identification.**

I. Introduction

HIGH-PERFORMANCE servo motor drives require appropriate control loop tuning for commissioning and regular operations to maintain a consistent dynamic response. They generally consist of current, velocity, and position control loops. To reduce setup time and prevent errors in manual tuning, various automatic control loop tuning schemes have been proposed in recent years. These methods are classified as offline and online methods. Most of them identify mechanical and/or electrical parameters during the tuning process. Establishing all of the controllers within a short time is crucial for the scheme to be acceptable in practice.

Numerous studies have proposed tuning the controllers on the basis of controller errors. For example, controller gains were adjusted continuously by using an adaptive rule and a velocity control error under various system parameter conditions [1]. A predetermined gain modifier calculated on the basis of the controller errors was used to adjust controller gains [2]. In addition, a model reference adaptive control was applied for gain tuning on the basis of controller output [3]. Although these methods do not require knowledge of motor parameters in general, complex control laws are involved in the tuning process, and therefore, a long execution time is often required. Furthermore, estimators have commonly been used for automatic tuning of controller gains. A sequential tuning method based on flux linkage, disturbance, and motor inertia estimators was proposed in [4]. The tuning requires several trapezoidal velocity cycles for converging the gains. Moreover, the controller settling time and overshoot were used as the weighting factors for loop gain tuning [5]. This scheme requires estimation of motor inertia and can be applied to an elastically connected load. A disturbance observer was also used for automatic control gain tuning [6]; however, in this study, only the position and velocity controllers were considered. In addition, a fuzzy-based scheme was used to tune the controller gains [7]. Both the controller following error and overshoot were used as the objective functions in this scheme. The aforementioned methods are generally complex, and a stable initial setup is often required to assure stable operation of the controllers.

Compared with online methods, offline methods can be executed in a shorter time, and motor parameters are essential to the tuning process. Least squares and signal injection was proposed as an offline method for identifying motor parameters and tuning current and speed loops [8]. Although electrical parameters can be calculated in a short time, the proposed method requires a stable initial tuning to measure mechanical parameters. Similarly, a tuning method based on the measurement of motor parameters and Taguchi methods was proposed in induction motor drives [9]. In this paper, motor torque constant was neglected, which renders the tuning scheme less practical. Another scheme proposed for tuning the control gains was based on step responses from various tests [10]. However, only the current controller was considered in this research.

Motor parameters are crucial for autotuning controllers. Although numerous parameter identification schemes have been proposed, they are used for purposes other than control loop tuning, such as estimating parameters for sensorless permanent-magnet synchronous motor drive control [11], [12], observers for controller compensation [13]–[15], and monitoring motor operating conditions [16]–[18].

This paper presents a simple but effective offline autotuning scheme for both of the current and motion controllers of permanent-magnet ac (PMAC) servo motor drives. Motor electrical parameters were identified first for current control loop tuning. The torque constant and mechanical parameters were then identified for velocity and position loop tuning. Compared

Manuscript received June 9, 2015; revised September 11, 2015; accepted October 8, 2015. Date of publication October 27, 2015; date of current version February 8, 2016. This work was supported by the Ministry of Science and Technology, Taiwan, under Grant MOST 103-2221-E-027-043-MY2.

S.-M. Yang is with National Taipei University of Technology, Taipei 10608, Taiwan (e-mail: smyang@ntut.edu.tw).

K.-W. Lin is with Lite-On Technology Corporation, Taipei 11492, Taiwan (e-mail: ghjpr10@gmail.com).

Color versions of one or more of the figures in this paper are available online at http://ieeexplore.ieee.org.

Digital Object Identifier 10.1109/TIE.2015.2495300

with existing offline autotuning schemes [8]–[10], the proposed scheme is more practical because it involves tuning all of the control loops in the motor drive.

The remainder of this paper is organized as follows. Section II presents the mathematical model of a PMAC motor. Section III details the design method for the control loops. The parameter estimation and related autotuning process are illustrated in Sections IV and V, respectively. Finally, Sections VI and VII present the experimental results and discussions, respectively.

II. Mathematical Model

The voltage equations of a three-phase PMAC motor in rotor reference frame can be expressed as

$$v_{qs}^r = (r_s + L_{qs}s)i_{qs}^r + \omega_r L_{ds} i_{ds}^r + \omega_r \lambda_m \tag{1}$$

$$v_{ds}^r = (r_s + L_{ds}s)i_{ds}^r - \omega_r L_{qs} i_{qs}^r \tag{2}$$

where v_{qs}^r, v_{ds}^r, i_{qs}^r, and i_{ds}^r are the q- and d-axis voltages and currents; r_s is the resistance; L_{qs} and L_{ds} are, respectively, the q- and d-axis inductances; λ_m is the flux linkage established by the rotor permanent magnets; ω_r is the rotor electrical speed; and "s" represents the Laplace operator. From (1), the back EMF constant can be expressed as $K_e = (P/2)\lambda_m$, where P is the number of rotor poles. The generated motor torque is

$$T_e = \frac{3}{2}\frac{P}{2}\left[\lambda_m i_{qs}^r + (L_{ds} - L_{qs}) i_{qs}^r i_{ds}^r\right]. \tag{3}$$

From (3), motor currents can be set to follow a trajectory for achieving maximum torque per ampere or other types of control. However, in this study, there is no need to run the motor at these modes, and the d-axis current was set to zero for convenience. Therefore, T_e is proportional to the q-axis current, and the motor torque constant is expressed as follows:

$$K_t = \frac{3}{2}\frac{P}{2}\lambda_m = \frac{3}{2}K_e. \tag{4}$$

The mechanical equation can be expressed as follows:

$$T_e = J\frac{d\omega_m}{dt} + B\omega_m + T_L \tag{5}$$

where J is the combined rotor and load inertia, B is the viscous frictional coefficient, ω_m is the mechanical speed, and T_L is the disturbance load torque.

III. Control System

Servo motor drives generally consist of two inner current control loops (q- and d-axes), a speed control loop, and an outer position control loop. Fig. 1 shows the schematic of the control system, where conventional linear regulators are used in the controllers. The path in the velocity loop with the differential "s" operator is generally realized with velocity command. The combined position and velocity loops represent a proportional-integral-derivative type position controller. Trapezoidal integration and simple difference are used for discretization of the controllers. The methods for determining the controller gains are described as follows.

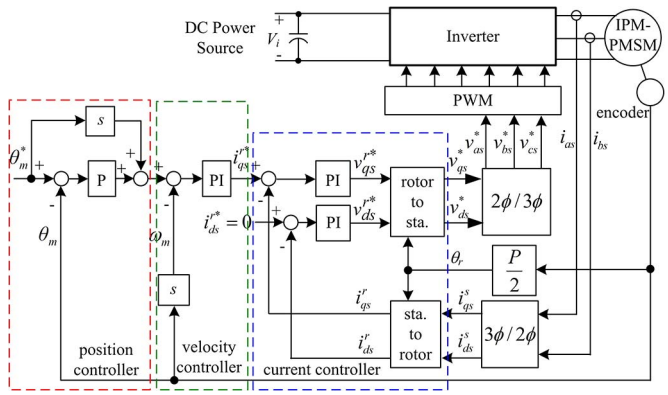

Fig. 1. Motor control system.

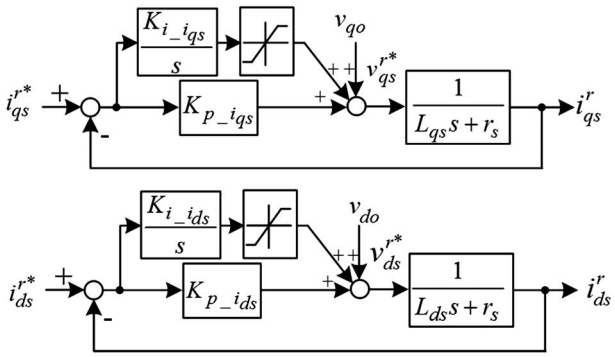

Fig. 2. q- and d-axis current controllers.

A. Current Controller

The schematics of the q- and d-axis current controllers are shown in Fig. 2; proportional plus integral (PI) regulators are used for control. Integrator voltages are limited to approximately half of the rated phase voltage. The cross-coupling voltages and the back EMF voltages are decoupled using the estimated electrical parameters and rotor speed. The decoupling voltages (i.e., v_{qo} and v_{do}) can be derived from (1) and (2) as

$$v_{qo} = \omega_r L_{ds} i_{ds}^r + \omega_r \lambda_m \tag{6}$$

$$v_{do} = -\omega_r L_{qs} i_{qs}^r. \tag{7}$$

For convenience, the gains of the current controllers are designed for the ratio between the proportional and integral gains to cancel out the $r_s - L$ pole. For example, in the q-axis, the gain ratio is set as follows: $K_{p\_i_{qs}}/K_{i\_i_{qs}} = L_{qs}/r_s$, where $K_{p\_i_{qs}}$ and $K_{i\_i_{qs}}$ are the proportional and integral gains, respectively. After the cancellation, the q-axis closed-loop transfer function can be simplified to

$$\frac{i_{qs}^r(s)}{i_{qs}^{r*}(s)} = \frac{\frac{K_{p\_i_{qs}}}{L_{qs}}}{s + K_{p\_i_{qs}}/L_{qs}} = \frac{\omega_{iq}}{s + \omega_{iq}} \tag{8}$$

where ω_{iq} is the cutoff of the q-axis current controller. Its value can be set according to the desired response. In general, the

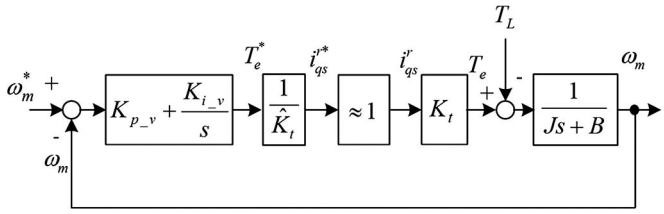

Fig. 3. Simplified velocity control loop.

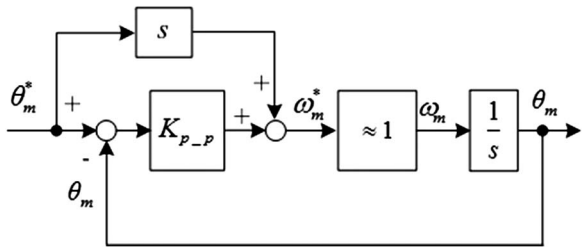

Fig. 4. Simplified position control loop.

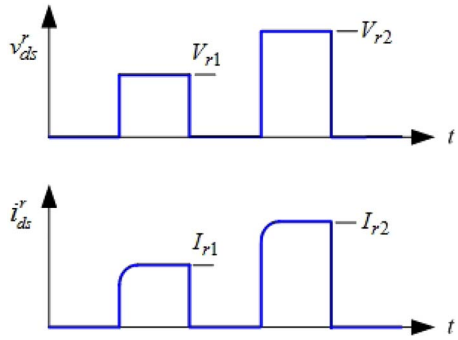

Fig. 5. Voltage and current waveforms when measuring resistance.

bandwidth of the current loop should be ten times the velocity loop bandwidth. The gains can then be expressed as follows:

$$K_{p\_i_{qs}} = \omega_{iq} \cdot L_{qs} \tag{9}$$

$$K_{i\_i_{qs}} = \omega_{iq} \cdot r_s. \tag{10}$$

The d-axis gains can be similarly determined. From the aforementioned equations, r_s, L_{qs}, and L_{ds} are required for calculating current controller gains.

B. Velocity Controller

As shown in Fig. 1, the velocity and position control loops cascade. Because the bandwidth of the current loop is higher than that of the velocity and position control loops, perfect current regulation was assumed for velocity control loop tuning. Fig. 3 shows the simplified velocity control system.

Let K_{p_v} and K_{i_v} be the proportional and integral gains of the velocity controller, respectively. The gain ratio is set as follows: $K_{p\_v}/K_{i\_v} = J/B$; then, the velocity control system can be expressed as

$$\frac{\omega_m(s)}{\omega_m^*(s)} = \frac{\frac{K_{i\_v}}{B}}{s + K_{i\_v}/B} = \frac{\omega_v}{s + \omega_v} \tag{11}$$

where ω_v is the cutoff frequency of the control system. The gains can be determined as follows:

$$K_{p\_v} = \omega_v \cdot J \tag{12}$$

$$K_{i\_v} = \omega_v \cdot B. \tag{13}$$

Because ω_v is set according to the desired bandwidth, J and B are required for calculating the velocity control loop gains. In addition, as shown in Fig. 3, torque constant (K_t) is required for the conversion between torque command (T_e^*) and current command (i_{qs}^{r*}).

C. Position Controller

Similarly, assuming that the bandwidth of the velocity control loop is much higher than that of the position control loop, the position control system can be simplified to Fig. 4. In actual implementation, the feedforward path will be neglected for convenience; therefore, the position control system can be expressed as

$$\frac{\theta_m(s)}{\theta_m^*(s)} = \frac{K_{p\_p}}{s + K_{p\_p}} \tag{14}$$

where K_{p_p} is the gain and the bandwidth of the control loop and is set according to the desired cutoff frequency of the position control system.

IV. Electrical Parameter Identification

As explained in Section III, resistance, inductances, and torque constant are required for tuning control loops. The identification procedures for these parameters are described as follows.

A. Stator Resistance (r_s)

To avoid error caused by rotor movements, resistance is measured by applying a d-axis voltage pulse (V_r). The steady-state d-axis current is then measured (I_r), and the resistance can be calculated as

$$r_s = \frac{V_r}{I_r}. \tag{15}$$

The rotor does not move with the aforementioned operation because the voltage pulse is short, and no q-axis current is produced.

In implementing the proposed scheme, two consecutive d-axis voltage pulses were applied to the motor to compensate for the error caused by the power switches and diode voltage drops. As shown in Fig. 5, these voltage pulses had the same polarity but different magnitudes. The resistance is calculated as

$$\hat{r}_s = \frac{V_{r2} - V_{r1}}{I_{r2} - I_{r1}} \tag{16}$$

where V_{r1} and V_{r2} are the voltage commands for the resistance estimation and $\hat{r}_s$ represents the measured or estimated value.

Note that the error caused by the power switches and diode voltage drops canceled out in (16).

B. Inductances (L_{ds}, L_{qs})

The inductances are measured by applying voltage pulses to the q- and d-axes, and the peak currents are then measured for calculating the inductances. Because the time duration for these voltage pulses is considerably short, typically less than 100 μs, the resistance drop and motor movements are neglected. With the assumption that the rotor is already aligned, from (1) and (2), motor voltages can be approximated as

$$v_{qs}^r \cong L_{qs} \cdot s \cdot i_{qs}^r \tag{17}$$

$$v_{ds}^r \cong L_{qs} \cdot s \cdot i_{ds}^r. \tag{18}$$

Because the current magnitude and generated torque are small, critical measurement errors may occur if the rotor movement is excessive. To reduce rotor movement, the time duration of the d-axis pulse is set to double that of the q-axis pulse. Let the width of the q- and d-axis pulses be h and $2h$, respectively; the inductances can be approximated as follows:

$$\hat{L}_{qs} \approx \frac{v_{qs}^r}{\Delta i_{qs}^r}\Delta t = \frac{V_{L\_q}}{I_{L\_q}}h \tag{19}$$

$$\hat{L}_{ds} \approx \frac{v_{ds}^r}{\Delta i_{ds}^r}\Delta t = \frac{V_{L\_d}}{I_{L\_d}}2h \tag{20}$$

where V_{L_q} and V_{L_d} are the magnitudes of the q- and d-axis voltage pulses, respectively, and I_{L_q} and I_{L_d} are the measured peak q- and d-axis currents, respectively.

Similar to resistance measurement, to reduce the errors caused by the inverter circuits, the aforementioned test is repeated twice with the same polarity but different magnitude voltage pulses. The differential voltage and current from these two tests are used for inductance calculations as follows:

$$\hat{L}_{qs} \cong \frac{V_{L\_q2} - V_{L\_q1}}{I_{L\_q2} - I_{L\_q1}}h \tag{21}$$

$$\hat{L}_{ds} \cong \frac{V_{L\_d2} - V_{L\_d1}}{\Delta i_{L\_d2} - I_{L\_d1}}2h \tag{22}$$

where the subscripts "1" and "2" represent the test number. Fig. 6 shows the schematic of the voltage and current waveforms for inductance measurement. After the resistance and inductances are measured, the current controller gains can be calculated using (9) and (10).

C. Feedforward Voltage and Torque Constant (v_{qo}, v_{do}, K_t)

Although the resistance and inductance measurements are static, the rotor must move to measure the feedforward voltages, torque constant, and mechanical parameters. Fig. 7 shows the theoretical currents and speed waveforms for these measurements. The current controller gains are set at $t = t_0$. A constant q-axis current command i_1 is then applied, and i_{ds}^r is set to 0. Because of the integrator limiter in the current controller, i_{qs}^r

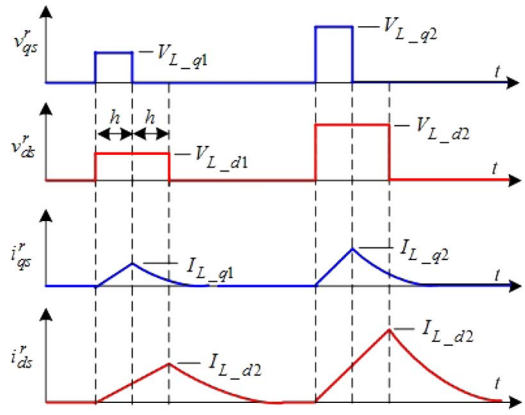

Fig. 6. Voltage and current waveforms when measuring inductances.

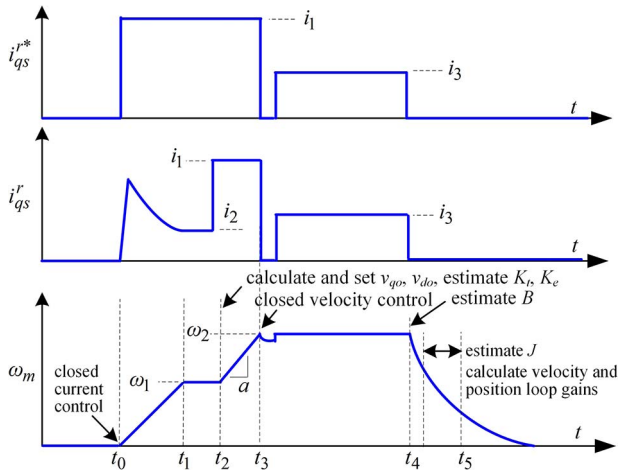

Fig. 7. Waveforms when measuring K_e, K_t, J, and B.

first increases and then decreases to a value i_2 as the speed settles at ω_1. Note that ω_1 is approximately half of the rated speed because the integrator voltages are limited to half of the rated phase voltage. After i_{qs}^r reaches a steady state, the permanent-magnet flux $\hat{K}_e$ can be estimated as

$$\hat{K}_e = \frac{P}{2}\hat{\lambda}_m = \frac{v_{qs}^{r*} - i_{qs}^r(\hat{L}_{qs} \cdot s + \hat{r}_s)}{\omega_m} \tag{23}$$

where v_{qs}^{r*} is the q-axis voltage command. The torque constant can then be calculated using $\hat{K}_t = 3/2\hat{K}_e$. In addition, the decoupling voltages, v_{qo} and v_{do}, can be calculated using (6) and (7).

At $t = t_2$, v_{qo} and v_{do} are established in the current controller. Because of the addition of these voltages, the current tracking error decreases to near zero, and the motor accelerates.

V. Mechanical Parameter Identification

At $t = t_3$, when the motor speed reaches a preset speed ω_2, the current command is set to zero for a short period of time to end the acceleration, the speed control loop is then closed, and the command is set to ω_2. The speed controller gains are set according to (12) and (13) with the estimated torque constant

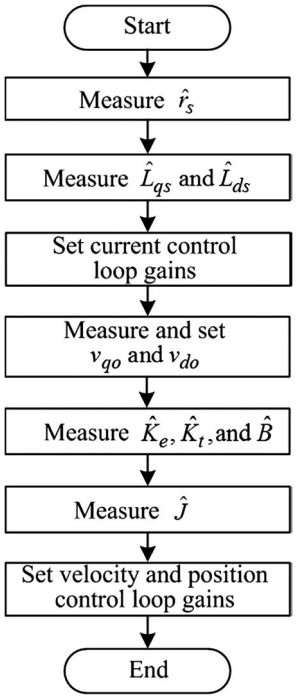

Fig. 8. Flowchart of the autotuning process.

$\hat{K}_t$ and an initial inertia $\hat{J}_o$. The variable B is set to zero in the calculations. The initial inertia is calculated as follows:

$$\hat{J}_o = \frac{\hat{K}_t i_1}{a} \tag{24}$$

where a is the acceleration rate between t_2 and t_3. The initial inertia $\hat{J}_o$ is an approximation only because the current is noisy and B is neglected. However, it can still facilitate tuning of an approximated speed controller for the rotor to reach a steady-state speed quickly. The experimental results showed that the motor may oscillate for a period if the speed loop gains are set arbitrarily. Consequently, the autotune process consumes more time.

During $[t_3, t_4]$, average i_{qs}^r is calculated and denoted as i_3. As shown in Fig. 7, at $t = t_4$, the motor reached a steady-state speed. Therefore, B can be calculated as

$$\hat{B} = \frac{\hat{K}_t \cdot i_3}{\omega_2}. \tag{25}$$

After the estimation of B, all of the controllers were switched off, and the motor decelerated down to zero speed. The motor speed in this region can be expressed as

$$\omega_m = \omega_2 \cdot e^{-\frac{\hat{B}}{\hat{J}}t}. \tag{26}$$

Therefore, motor inertia can be calculated using the velocity waveform during the $[t_4, t_5]$ region through curve fitting.

The inertia calculated using curve fitting is more accurate than $\hat{J}_o$ because it is less sensitive to measurement noise. After $\hat{J}$ and $\hat{B}$ were measured, the velocity and position control gains were calculated using (10)–(12). The autotune process was thus completed, and the motor drive was ready for servo operations. Fig. 8 shows the flowchart for parameter identification and the controller gain tuning process.

TABLE I
COMPARISONS OF MANUAL AND AUTOIDENTIFIED PARAMETERS

	Manual	Auto-identified	% Error
r_s (Ω)	2.7	2.89	6.3%
L_{qs} (mH)	5.5	4.99	9.2%
L_{ds} (mH)	4.67	5.25	11%
J (kg-m^2)	3.28x10^{-4}	3.44x10^{-4}	5%
B (Nm/rad/s)	2.33x10^{-3}	2.45x10^{-3}	5.1%
K_t (Nm/A)	0.486	0.478	1.5%

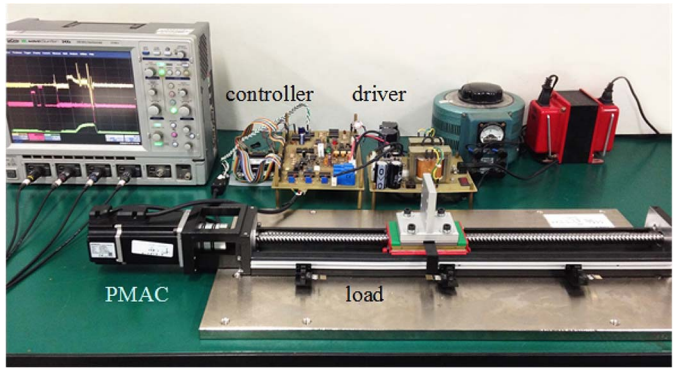

Fig. 9. Experimental system.

VI. EXPERIMENTAL RESULTS

A 400-W 8-pole PMAC was used for experimental verification of the proposed autotune scheme. Motor controllers were implemented with a digital signal processor. The sampling frequency for the current controller is 18 kHz, and it is 2.2 kHz for the velocity and position control loops. SPWM was employed for voltage modulation. The manually measured motor parameters are listed in Table I. The magnitudes of the voltage pulses used for resistance measurement were 3.1 and 4.8 V, respectively, and each pulsewidth was 62.5 ms. The magnitudes of the voltage pulses for q-axis inductance measurement were 25 and 50 V, those of the d-axis were 21 and 42 V, respectively, and the pulsewidth $h = 55$ μs. The cutoff frequencies of the current loop (ω_{iq} and ω_{id}), velocity loop (ω_v), and position loops were set to 600, 30, and 6 Hz, respectively. Fig. 9 shows the experimental system.

Fig. 10 shows the q- and d-axis currents and the speed waveforms for the autotune process. Fig. 11 shows the amplified view of the r_s and L measurement waveforms shown in Fig. 10. The two larger square pulses are the resistance measuring pulses, and the two smaller pulses are the inductance measuring pulses. As shown in these figures, r_s, L_{qs}, and L_{ds} measurements take approximately 0.3 s. Fig. 12 shows an amplified view of the K_t, J, and B measurement waveforms shown in Fig. 10. The motor drive actions are denoted at the top of the figure. As described in Section IV, v_{qo} and v_{do} were calculated and established in the controller during the constant current control period. In addition, $\hat{K}_t$ was estimated during this period. The initial moment of inertia $\hat{J}_o$ was calculated after the motor reached the target speed. The torque constant

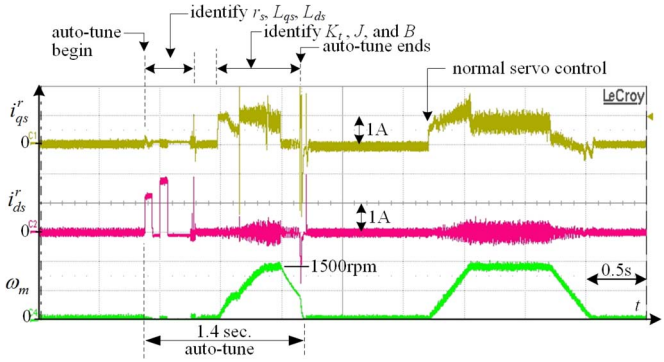

Fig. 10. Motor q- and d-axis currents and speed waveforms for the autotuning process; target speed $= 1500$ r/min.

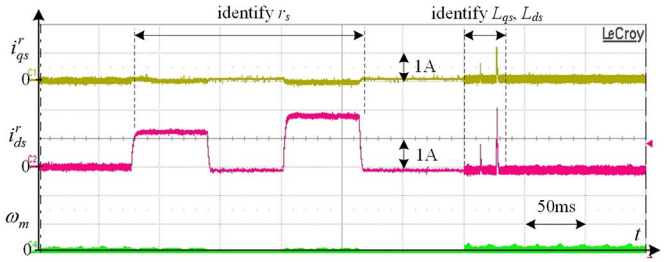

Fig. 11. Amplified view of the r_s, L_{qs}, and L_{ds} measurements shown in Fig. 10.

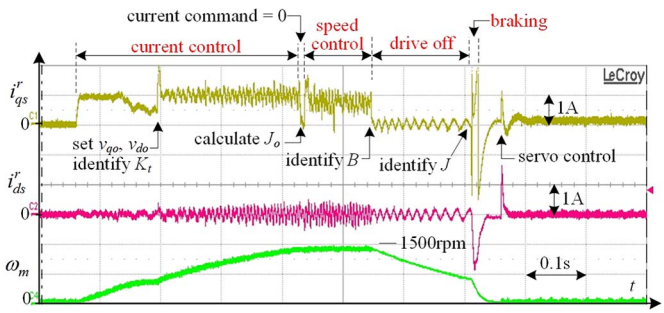

Fig. 12. Amplified view of the K_t, J, and B measurements shown in Fig. 10.

$\hat{K}_t$ and initial moment of inertia $\hat{J}_o$ were then used for tuning the speed controller, which was then activated. The motor speed reached a steady state shortly after the controller was closed. At the end of the speed control period, $\hat{B}$ was calculated. The motor drive was then turned off for the final measurement of the moment of inertia. The drive was set to braking mode after the inertia was measured. The position and velocity controller gains were then calculated, and the drive was ready for servo control. Fig. 13 shows the instantaneous estimated $\hat{K}_t$, $\hat{B}$, and $\hat{J}$ during the autotune process. The moment of inertia J_o differs considerably from the final measured $\hat{J}$ primarily because of measurement noises and the frictional torque being neglected when calculating $\hat{J}_o$. The entire autotune process takes approximately 1.4 s for completion.

Fig. 14 shows the same waveforms as those shown in Fig. 10, except that the target speed was set to 750 r/min. The autotune process runs similarly to that shown in Fig. 10. The

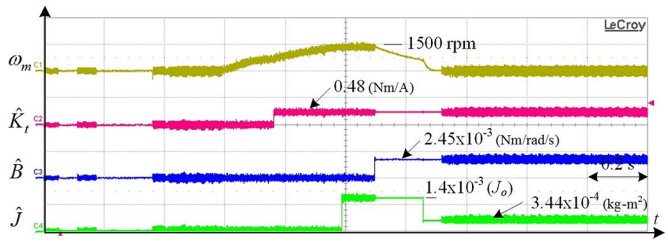

Fig. 13. Motor velocity and the instantaneous estimated K_t, B, and J during autotune.

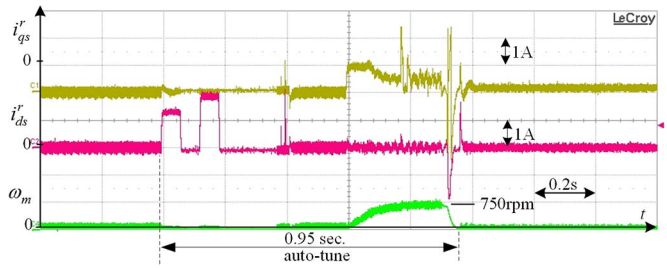

Fig. 14. Motor q- and d-axis currents and speed waveforms for the autotuning process; target speed $= 750$ r/min.

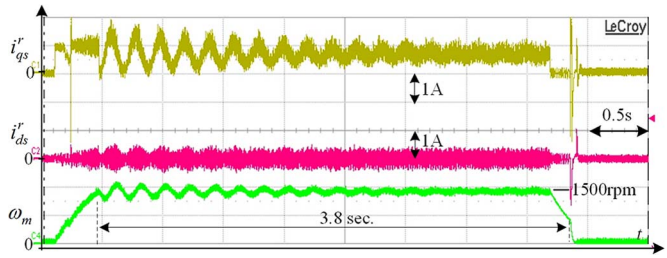

Fig. 15. Motor q- and d-axis current and speed waveforms for the autotuning process; K_{p_v} and K_{i_v} during $[t_3, t_4]$ are set to 0 and 1, respectively.

tuning process took less time to complete than that shown in Fig. 10 because motor speed converged faster. In addition, as mentioned in Section V, improper setting of K_{p_v} and K_{i_v} during $[t_3, t_4]$ may increase the tuning time. Fig. 15 shows the waveforms when K_{p_v} and K_{i_v} were set to arbitrarily selected values of 0 and 1, respectively. The motor oscillated in the constant speed control region. Therefore, a longer time was required to complete the tuning process.

To verify the performance of the system tuned using the proposed method, the closed-loop frequency responses of the q-axis current, velocity, and position controls were measured, as shown in Figs. 16–18, respectively. The current response was consistent with the tuning when the cutoff frequency was set to 600 Hz. The velocity frequency response revealed a bandwidth of approximately 55 Hz, as expected. In addition, the -3-dB point of the position response was approximately 6 Hz, which is the designed bandwidth of the controller. Fig. 19 presents the step response of the q-axis current control. The rising time was approximately 600 μs. Because of the current limitation, the velocity control was tested under its maximal acceleration rate, and the response is shown in Fig. 20. The q-axis current

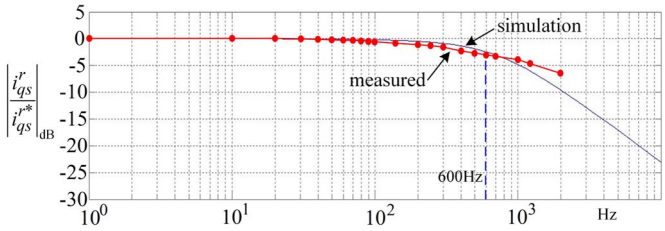

Fig. 16. Measured closed-loop frequency response of the q-axis current control loop.

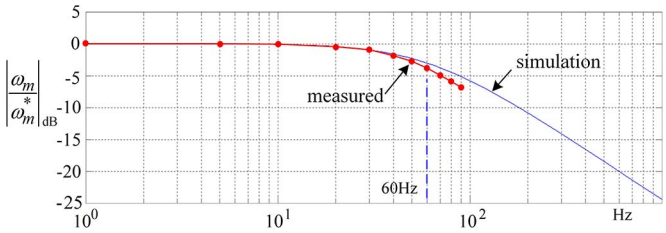

Fig. 17. Measured closed-loop frequency response of the velocity control loop.

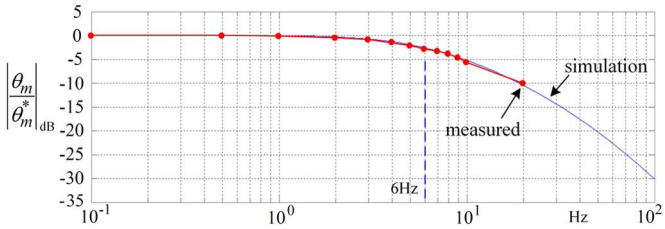

Fig. 18. Measured closed-loop frequency response of the position control loop.

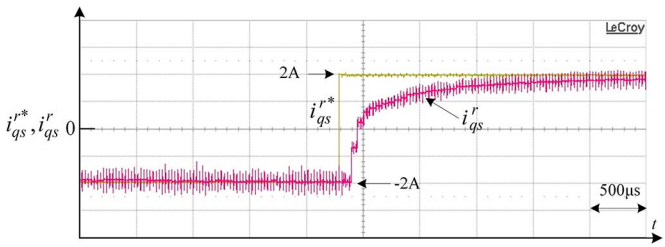

Fig. 19. Step response of the q-axis current control loop.

was approximately 3 A during the acceleration period. Fig. 21 shows the position loop response when a sinusoidal position command was applied. The magnitude of the motor position was attenuated to 0.707 times the position reference when the frequency was 6 Hz. Fig. 22 depicts the response of the rated load torque when the motor was running at 1000 r/min, indicating that the disturbance was rejected successfully and that the motor speed returned to its original speed within 0.3 s.

A comparison of the parameters measured in the proposed scheme with the manual measurements is shown in Table I. Five measurements were performed and averaged. In addition, the percentage errors between the manual and autoidentified parameters are shown in the table with the manual values as

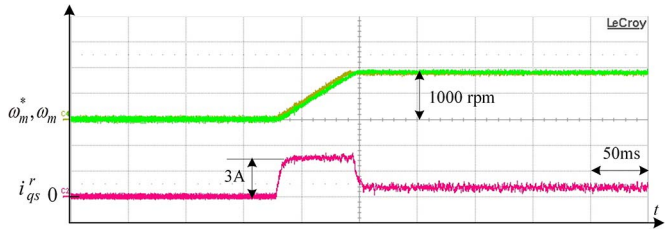

Fig. 20. q-axis current and speed response when the motor accelerated from 0 to 1000 r/min with the maximum drive current (3 A).

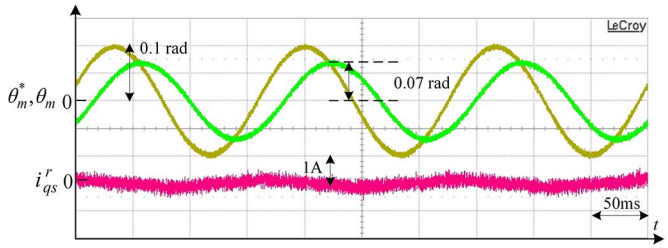

Fig. 21. q-axis current and position response when the motor was commanded with 6-Hz sinusoidal reference.

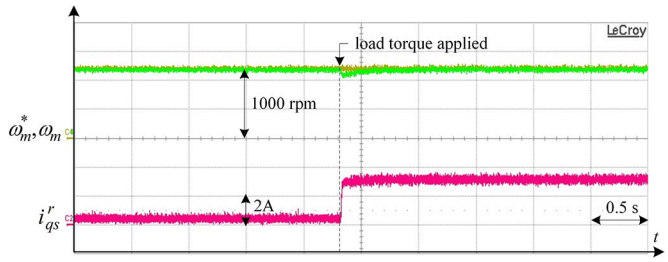

Fig. 22. q-axis current and speed response when the motor was running at 1000 r/min and step rated load torque was applied.

the basis. Most of the parameter errors are within 10%. Among them, inductances have the highest errors.

VII. Discussion of Results

The autotuning scheme presented in the previous sections integrates several simple techniques to estimate the required parameters and then tunes all of the control loops automatically. In our implementation of the scheme, most of the parameter estimation errors were within 10%, and inductances exhibited the largest errors. These errors might have been caused by variation in the supply voltage caused by the rapidly rising current during the measurements. Although resistance was neglected in the inductance calculations, its influence was small because the resistive drop was canceled out in the calculations.

As explained in Section V, the initial setting for K_{p_v} and K_{i_v} does not include frictional torque. Therefore, the tuning would be more overdamped in the presence of friction in an actual system. Consequently, an unstable condition is unlikely to occur; if it does, then other tuning methods should be used.

In the experimental verification, we set the cutoff frequencies of the current loop, velocity loop, and position loop to 600, 30, and 6 Hz, respectively. The corresponding bandwidth of these

loops would be approximately the cutoff frequency set for that loop. Both the closed-loop frequency and transient responses were consistent with the tuning. These results indicate that, even with some minor errors in the estimated parameters, the autotuning process can deliver the desired dynamic responses.

VIII. Conclusion

An automatic tuning scheme for the controllers of PMAC servo motor drives has been presented in this paper. Depending on the parameter to be identified, the controller sends out appropriate signals to the motor drive for measurement. The control loop gains are tuned automatically with the identified parameters. The experimental results verified that the proposed scheme can estimate parameters accurately. Furthermore, depending on the setting of the tuning process, it can be completed within 1.4 s. The control system tuned using the proposed scheme can achieve strong dynamic performance. In addition, the system tuned using the proposed scheme is consistent with the desired dynamic performance according to the measured frequency response.

References

[1] J. W. Jung, V. Q. Leu, T. D. Do, E. K. Kim, and H. H. Choi, "Adaptive PID speed control design for permanent magnet synchronous motor drives," *IEEE Trans. Power Electron.*, vol. 30, no. 2, pp. 900–908, Feb. 2015.

[2] D. Simhachalam, C. Dey, and R. K. Mudi, "An auto-tuning PD controller for dc servo position control system," in *Proc. IEEE Power, Control Embedded Syst. Conf.*, 2012, pp. 1–6.

[3] T. Higashiyama *et al.*, "Auto-tuning of motor drive system by simple adaptive control approach," in *Proc. IEEE Control Appl. Int. Conf.*, Sep. 2000, pp. 868–873.

[4] K. H. Kim, "Nonlinear speed control for a PM synchronous motor with a sequential parameter auto-tuning algorithm," *IEEE Trans. Power Electron.*, vol. 152, no. 5, pp. 1253–1262, May 2005.

[5] M. Calvini, M. Carpita, A. Formentini, and M. Marchesoni, "PSO-based self-commissioning of electrical motor drives," *IEEE Trans. Ind. Electron.*, vol. 62, no. 2, pp. 768–776, Feb. 2015.

[6] S. M. Yang and Y. J. Deng, "Observer-based inertial identification for auto-tuning servo motor drives," in *Conf. Rec. 40th IEEE IAS Annu. Meeting*, Oct. 2–6, 2005, pp. 968–972.

[7] K. Y. Cheng and Y. Y. Tzou, "Fuzzy optimization techniques applied to the design of a digital PMSM servo drive," *IEEE Trans. Power Electron.*, vol. 19, no. 4, pp. 1085–1099, Nov. 2004.

[8] D. Tadokoro, S. Morimoto, Y. Inoue, and M. Sanada, "Method for auto-tuning of current and speed controller in IPMSM drive system based on parameter identification," in *Proc. IEEE Power Electron. Conf.*, May 2014, pp. 390–394.

[9] Y. S. Lai, J. C. Lin, and J. J. Wang, "Direct torque control induction motor drives with self-commissioning based on Taguchi methodology," *IEEE Trans. Power Electron.*, vol. 15, no. 6, pp. 1068–1071, Nov. 2000.

[10] S. B. Lee, "Closed-loop estimation of permanent magnet synchronous motor parameters by PI controller gain tuning," *IEEE Trans. Energy Convers.*, vol. 21, no. 4, pp. 863–870, Dec. 2006.

[11] M. A. Hamida, J. De Leon, A. Glumineau, and R. Boisliveau, "An adaptive interconnected observer for sensorless control of PM synchronous motors with online parameter identification," *IEEE Trans. Ind. Electron.*, vol. 60, no. 2, pp. 739–748, Feb. 2013.

[12] M. Rashed, P. A. MacConnell, A. F. Stronach, and P. Acarnley, "Sensorless indirect-rotor-field-orientation speed control of a permanent-magnet synchronous motor with stator-resistance estimation," *IEEE Trans. Ind. Electron.*, vol. 54, no. 3, pp. 1664–1675, Jun. 2007.

[13] W. S. Huang, C. W. Liu, P. L. Hsu, and S. S. Yeh, "Precision control and compensation of servomotors and machine tools via the disturbance observer," *IEEE Trans. Ind. Electron.*, vol. 57, no. 1, pp. 420–429, Jan. 2010.

[14] S. Li and Z. Liu, "Adaptive speed control for permanent-magnet synchronous motor system with variations of load inertia," *IEEE Trans. Ind. Electron.*, vol. 56, no. 8, pp. 3050–3059, Aug. 2009.

[15] T. Boileau, N. Leboeuf, B. Nahid-Mobarakeh, and F. Meibody-Tabar, "Online identification of PMSM parameters: Parameter identifiability and estimator comparative study," *IEEE Trans. Ind. Appl.*, vol. 47, no. 4, pp. 1944–1957, Jul./Aug. 2011.

[16] K. Liu, Z. Q. Zhu, and D. A. Stone, "Parameter estimation for condition monitoring of PMSM stator winding and rotor permanent magnets," *IEEE Trans. Ind. Electron.*, vol. 60, no. 12, pp. 5902–5913, Dec. 2013.

[17] T. L. Vandoorn, F. M. De Belie, T. J. Vyncke, J. A. Melkebeek, and P. Lataire, "Generation of multisinusoidal test signals for the identification of synchronous-machine parameters by using a voltage-source inverter," *IEEE Trans. Ind. Electron.*, vol. 57, no. 1, pp. 430–439, Jan. 2010.

[18] M. C. Chou and C. M. Liaw, "Dynamic control and diagnostic friction estimation for an SPMSM-driven satellite reaction wheel," *IEEE Trans. Ind. Electron.*, vol. 58, no. 10, pp. 4693–4707, Oct. 2011.

Sheng-Ming Yang (M'90) received the M.S. and Ph.D. degrees in mechanical engineering from the University of Wisconsin–Madison, Madison, WI, USA, in 1985 and 1989, respectively.

From 1989 to 1992, he was a Development Engineer with Unico Inc., and from 1992 to 1995, he was a Principal Engineer with the Corporate Technology Center, A. O. Smith Co., Milwaukee, WI. In 1995, he joined Tamkang University, Taipei, Taiwan, as a Professor with the Department of Mechanical and Electro-Mechanical Engineering. Since 2007, he has been with the Department of Electrical Engineering, National Taipei University of Technology, Taipei. His research interests are ac and dc motor drives and control.

Kuang-Wei Lin received the M.S. degree in electrical engineering from National Taipei University of Technology, Taipei, Taiwan, in 2015.

He then joined Lite-On Technology Corporation, Taipei, as an R&D Engineer. His research interests include ac motor drives and control.